Lab on a Chip

PAPER

View Article Online
View Journal | View Issue

Cite this: *Lab Chip*, 2024, **24**, 1996

Wearable intelligent sweat platform for SERS-AI diagnosis of gout†

Zhaoxian Chen,[a] Wei Wang,[a] Hao Tian,[a] Wenrou Yu,[a] Yu Niu,[a] Xueli Zheng,*[a] Shihong Liu,[b] Li Wang[c] and Yingzhou Huang *[a]

Received 19th December 2023,
Accepted 12th February 2024

DOI: 10.1039/d3lc01094e

rsc.li/loc

For the past few years, sweat analysis for health monitoring has attracted increasing attention benefiting from wearable technology. In related research, the sensitive detection of uric acid (UA) in sweat with complex composition based on surface-enhanced Raman spectroscopy (SERS) for the diagnosis of gout is still a significant challenge. Herein, we report a visualized and intelligent wearable sweat platform for SERS detection of UA in sweat. In this wearable platform, the spiral channel consisted of colorimetric paper with Ag nanowires (AgNWs) that could capture sweat for SERS measurement. With the help of photos from a smartphone, the pH value and volume of sweat could be quantified intelligently based on the image recognition technique. To diagnose gout, SERS spectra of human sweat with UA are collected in this wearable intelligent platform and analyzed by artificial intelligence (AI) algorithms. The results indicate that the artificial neural network (ANN) algorithm exhibits good identification of gout with high accuracy at 97%. Our work demonstrates that SERS-AI in a wearable intelligent sweat platform could be a feasible strategy for diagnosis of gout, which expands research on sweat analysis for comfortable and noninvasive health monitoring.

1. Introduction

The fast development of wearable sensors for comfortable and noninvasive diagnosis of diseases has attracted more and more attention in recent years.[1–3] Since sweat contains lots of biochemical metabolites as biomarkers of diseases including glucose,[4] urea,[5] uric acid (UA),[6] and metal ions,[7] the wearable sweat platform for health monitoring becomes[8] a famous star in related fields.[3] Among these biomarkers, uric acid is a typical analyte in sweat closely associated with gout.[9] In present studies, the electrochemical (EC) technique is mainly adopted to perform sweat analysis.[10] These EC sensors mainly rely on enzymes and antibodies as biorecognition elements to achieve specific quantification of metabolite and stress biomarkers in sweat, as shown in Table S1 in the ESI.†[9,11–15] However, enzymes and antibodies are prone to degrade over time and lose their functionality after exposure to harsh environments and contamination.

Surface Enhanced Raman Spectroscopy (SERS) is an ultrasensitive spectral analytical technique at the single molecule level,[16–18] which is wildly applied in various fields, including biological medicine,[19] chemical analysis,[20,21] *etc.* The great enhancement of the SERS signal is primarily attributed to the highly confined electromagnetic field induced by the collective oscillation of free electrons at the metal surface which is called surface plasmon.[18] Benefiting from the characteristic Raman peaks in the spectrum, SERS as an optical fingerprint with high sensitivity exhibits broad potential in sweat analysis for diagnosis of diseases.[22,23] Recently, researchers have developed flexible wearable SERS substrates using Ag nanocubes and polydimethylsiloxane (PDMS) to analyze trace amounts of drugs in sweat.[24] Additionally, the combination of paper microfluidics and plasmonic Au nanorods has been reported to quantify UA concentration in sweat.[25] Therefore, SERS detection and monitoring of UA in wearable sweat platforms could overcome the disturbance from complex compositions in human sweat to diagnose gout.

However, accurate identification of UA in human sweat with lots of complex compositions based on SERS spectra is still a great challenge in related studies. Recently, artificial intelligence (AI) algorithms have been adopted in analysis of SERS spectra and showed great value in the promotion of accuracy and efficiency, especially in diagnosis of diseases, including breast cancer,[26] prostate cancer,[27] lung cancer,[28] *etc.* Therefore, AI algorithm enabled SERS diagnosis of gout in a wearable sweat platform is performed in this work. Here

[a] *Chongqing Key Laboratory of Chongqing Key Laboratory of Interface Physics in Energy Conversion, College of Physics, Chongqing University, Chongqing, 400044, China. E-mail: zhengxueli0315@cqu.edu.cn, yzhuang@cqu.edu.cn*
[b] *Chongqing University Cancer Hospital, Department of Palliative care, Department of Geriatric Oncology, Chongqing, China*
[c] *Key Laboratory of Optoelectronic Technology and Systems (Ministry of Education), College of Optoelectronic Engineering, Chongqing University, Chongqing 400044, China*

† Electronic supplementary information (ESI) available. See DOI: https://doi.org/10.1039/d3lc01094e

a paper fluidics coated by Ag nanowires (AgNWs) with a spiral channel is the core component of this wearable platform. The AgNWs is designed to obtain SERS spectra of sweat as an enhanced substrate based on surface plasmon. And the spiral channel is fabricated to acquire the volume and pH value of sweat with the help of photos from a smartphone based on an image recognition technique. Our data demonstrate that this wearable platform could detect analyte in sweat with high sensitivity and intelligently quantify the volume and pH value of sweat. Based on the artificial neural network (ANN) algorithm, SERS identification of gout in simulated human sweat with complex compositions exhibits high accuracy at 97%. This innovative wearable SERS platform offers a noninvasive and high-sensitivity SERS detection method, which shows excellent potential for point-of-care (PoC) applications in health monitoring.

2. Materials and method

2.1 Preparation of the wearable sweat platform

All information of chemicals used in this work could be seen in the ESI.† The AgNWs were synthesized using a standard reported polyol method with some modification,[29,30] whose detailed process could be seen in the ESI.† The fabrication process of the wearable sweat platform is shown in Fig. S1 in the ESI.† Firstly, spired paper devices with a channel width of 2 mm were fabricated by engraving organic filter paper into a designed shape using a 100 W laser engraving machine (4060 laser engraving machine) with predesigned CorelDRAW 2019 patterns. The paper with a circuitous design serves as an effective microfluidic channel that transports the excreted sweat through the porous medium by wicking without the need for external force or inlet pressure. 100 μL of AgNWs solution was dropped onto the spired paper, which was followed by vacuum filtration for 1 minute. After that, the paper was dried for 10 minutes at 60 °C and coated with 20 μL bromocresol green pH indicator solution. Then, a mixture of PDMS and curing agent from the Sylgard 184 silicone elastomer kit was prepared in a 10 : 1 weight ratio and degassed under vacuum for 20 min. The PDMS mixture was spin-coated onto a silicon wafer at 500 rpm for 20s and dried for 30 min at 120 °C to create PDMS films. At last, the paper with AgNWs and PDMS was assembled on a medical-grade double-sided adhesive tape and then covered with a thin PDMS film.

2.2 Measurement of SERS spectra

The SERS spectra of each dye molecule were collected on a Raman spectrometer (iHR550, Horiba) with an exposure time of 5 s excited by a 632.8 nm laser. Human sweat samples were collected from thirteen volunteers with or without UA added. The Ethic Committee of College of Physics in Chongqing University approves all human experiments.

2.3 Analysis by artificial intelligence algorithms

Several artificial intelligence algorithms using the Keras library in Python were adopted to analyze SERS spectra of UA in human sweat. These algorithms included the linear discriminant analysis (PLS) algorithm, principal component analysis (PCA) algorithm, and artificial neural network (ANN) algorithm.

2.4 Quantification of the volume and pH value of sweat

The pH value and volume (travel distances in spiral channel) of sweat were qualified by a Python code. To minimize deviation in the photo process, the code loads the image of the sweat infiltration region, converts it to grayscale, thresholds it to create a binary image, finds the contours in the picture, and then selects the most prominent outline. This code could be modified to work with different images and to perform additional processing steps if needed.

3. Results and discussion

3.1 Structure of the wearable intelligent sweat platform

Fig. 1 shows the sketch of the wearable intelligent sweat platform, which is composed of several layers, including a double-sided medical adhesive, bottom PDMS layer, paper fluidic layer with AgNWs and top encapsulation PDMS layer. The bottom PDMS layer provides structural support, while the top encapsulation PDMS layer protects the device from external disturbance such as moisture and dust. Benefiting from the AgNWs on the paper fluidic layer, UA in human sweat could be detected and monitored by SERS (Fig. 1a). The scanning electron microscopy (SEM) images reveal the distribution of the AgNWs on the surface of the paper (Fig. S2a and b†), which has an average diameter of 0.195 ± 0.04 μm and an average length of 13.09 ± 5.05 μm as seen in Fig. S2c and d.† The absorption spectrum of the AgNWs solution shows a single plasmonic band with a peak position at 350 nm. Besides, the extinction distribution of AgNWs on the paper substrate is also confirmed (Fig. S2e and f†). Since the sweat needs to be extracted through the paper fluidic channel with the help of capillary action in this wearable platform, the influence of AgNWs on the surface wettability of paper is also discussed and shown in Fig. S3a and b.† These images indicate that the filter paper without and with AgNWs exhibits a contact angle of 25.33° and 22.97°, respectively, which demonstrates that this paper fluidic channel remains hydrophilic with AgNWs. Therefore, the volume and pH value of sweat could be further qualified on this wearable AgNW enhanced SERS platform with the help of smartphone photos and an image recognition technique.

3.2 SERS sensitivity of the wearable intelligent sweat platform

To discuss the SERS performance of this wearable intelligent sweat platform, SERS spectra of NB (Nile blue) at 10^{-7} M are collected and shown in Fig. 2a. The obvious Raman peak at

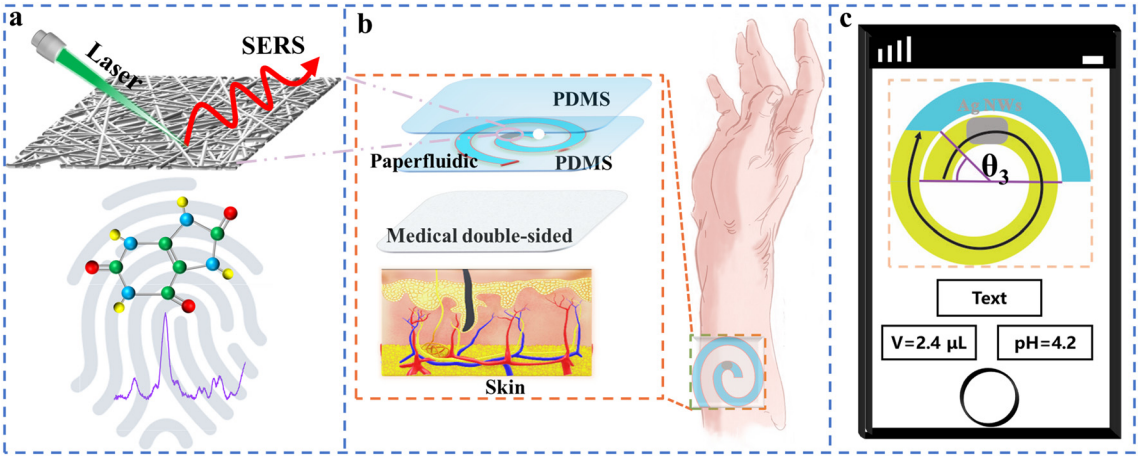

Fig. 1 The sketch and detection process of the wearable intelligent sweat platform. (a) SERS detection. (b) Various layers of the platform. (c) Smartphone interface of the quantified volume and pH value.

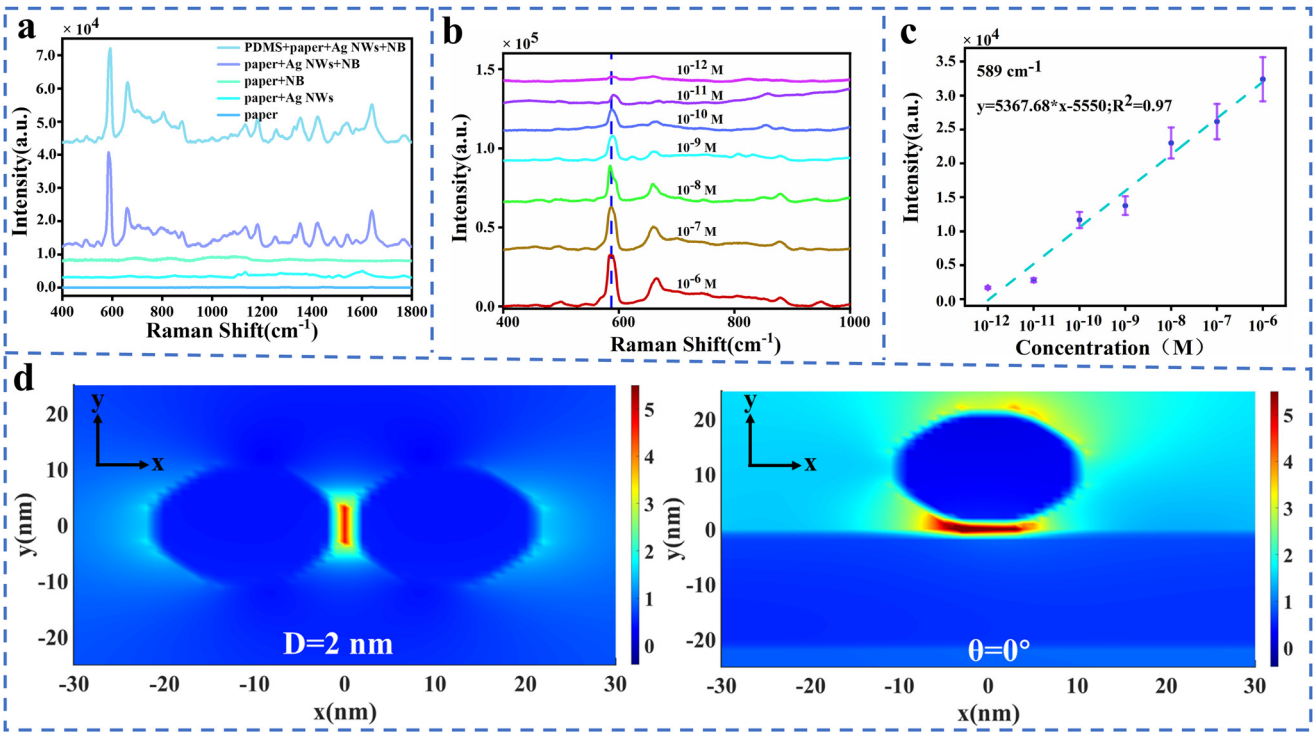

Fig. 2 SERS spectra (a) on various papers and (b) of NB with different concentrations; (c) the linear fitting curve of Raman intensities at 589 cm^{-1}; (d) simulated electric field distribution of the AgNW dimer.

589 cm^{-1} demonstrates the excellent SERS enhancement provided by AgNWs, whose enhancement factor (EF) is estimated to be 1.14×10^6 (detailed calculation shown in the ESI†). SERS spectra of NB with concentrations ranging from 1×10^{-6} M to 1×10^{-12} M are also obtained and shown in Fig. 2b. This experimental results demonstrate that our wearable intelligent sweat platform has a high SERS sensitivity at 1 pM, which has great advantage in the diagnosis of disease through sweat. Furthermore, the relationship between the concentration of NB and its characteristic Raman peak is also explored in Fig. 2c. The high coefficient (R^2 = 0.97) of linear fitting curve offers convenience in the analysis of SERS detection. To understand the huge SERS enhancement in this wearable intelligent sweat platform, the electric field distribution of AgNWs dimer is simulated based on the Finite-Difference Time-Domain (FDTD) method. In the FDTD model, the AgNWs have a 10 nm diameter and 10 μm length with 2 nm gap distance,[31] as shown in Fig. 2d. Fig. 2d and S4† show that the electric field enhancement is largely influenced by the

gap distance in nanowires dimer with parallel or vertical configuration. This means that the strong surface plasmon coupling between AgNWs dominates the SERS enhancement, which comes from the three-dimensional (3D) AgNW network shown in Fig. S2a and b.† Furthermore, our simulated data point out that the polarization of incident light has a slight effect on this surface plasmon coupling enhancement shown in Fig. S5.†[31] These simulated results are consistent with our experimental data, which indicates that the denser AgNWs generate a larger SERS enhancement due to the hotter spot formed by the AgNW dimer with a tiny gap. In addition to this, this work also investigates the effect of different diameters and lengths of silver nanowires on the electric field strength, as shown in Fig. S6.†

To investigate the detection performance of this wearable platform, the SERS uniformity in space and time is discussed here. Firstly, SERS spectra of NB at 10^{-7} M are collected at 15 randomly selected points on the paper fluidic channel with AgNWs, whose Raman intensities varied within a range of 5% shown in Fig. S7a and b in the ESI.† And then Raman mapping with an area of 25 μm × 25 μm is performed on this SERS substrate, whose intensities of Raman peak at 589 cm^{-1} exhibit low RSD at 2.26% as shown in Fig. S7c and S6d in the ESI.† Finally, the stability of this SERS substrate is investigated by continuously collecting SERS spectra for 8 days as shown in Fig. S7e,† whose RSD of Raman intensities at 589 cm^{-1} is 4% with a slight decrease as shown in Fig. S6f.† In addition, the thickness of the PDMS encapsulation layer also affects the SERS spectral intensity. As the PDMS thickness increases from 160 μm to 320 μm, the SERS spectral intensity exhibits a 37% increase (Fig. S8†). We chose a PDMS film with a thickness of 200 μm as the encapsulation layer to ensure conformal contact with the paper microfluidic channel while minimizing sweat evaporation. These experimental results demonstrate that our wearable sweat platform with AgNWs is a reliable SERS substrate for the detection and monitoring of trace substances.

3.3 SERS spectra of UA in synthetic sweat

To diagnose gout based on UA in human sweat, the SERS spectra of UA in synthetic sweat are firstly investigated. Fig. 3a illustrates SERS spectra of UA with concentration ranging from 1×10^{-3} M to 1×10^{-7} M, which exhibits the high SERS sensitivity of this wearable sweat platform at 10^{-7} M. The resulting SERS spectra were analyzed to determine the limit of detection and sensitivity of the SERS platform for UA detection. The C–N stretching vibration of UA is responsible for the peak observed at 496 cm^{-1}. These peaks are consistent with those measured from UA powder as shown in Fig. S9.† Fig. 3b shows the relationship between the concentration of UA and corresponding SERS intensity, which demonstrates the exceptional detection capability of this platform for SERS detection of UA in synthetic sweat. Because of the complex components in human sweat, the selectivity of this wearable platform for SERS detection of UA is also studied. To evaluate the specificity of UA detection against other biomolecules, the wearable sweat platform was exposed to various potential interfering molecules, including sodium

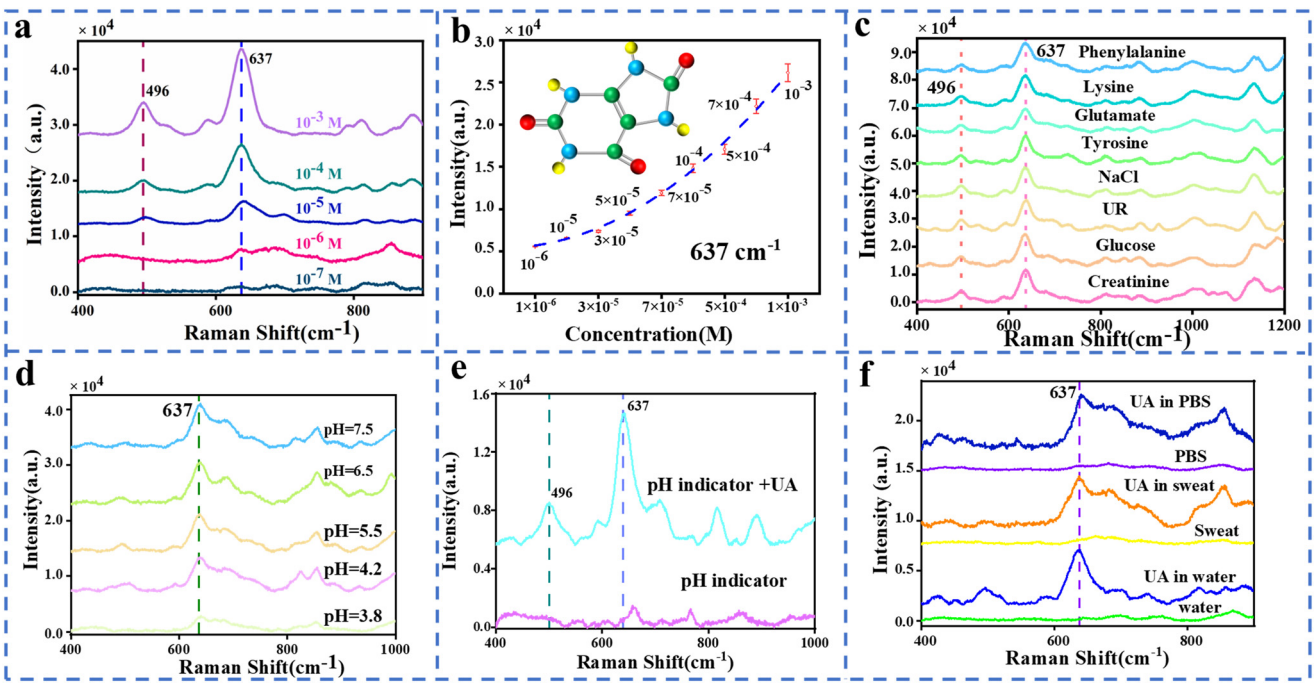

Fig. 3 (a) SERS spectra of UA with different concentrations. (b) The polynomial fitting curve of SERS intensity at 637 cm^{-1}. (c) SERS spectra of UA with other analytes. (d) SERS spectra of UA in sweat with different pH values. (e) SERS spectra of UA with a pH indicator. (f) SERS spectra of UA in various environments.

chloride, glucose, creatinine, urea, tyrosine, glutamate, lysine, and phenylalanine (Fig. 3c and S10†). The SERS spectra of these interfering molecules confirmed the absence of a UA Raman characteristic peak at 637 cm^{-1}. Therefore, their presence in sweat would not affect the accuracy of UA detection.

Moreover, SERS spectra of UA at 10^{-4} M in various ambient environments are also presented in Fig. 3. The obvious characteristic Raman peak of UA at 637 cm^{-1} is shown in SERS spectra collected in synthetic sweat with various pH values or pH indicators as shown in Fig. 3d and e, which means that the SERS detection of UA is compatible with the detection of the pH value of sweat in our wearable platform. The SERS spectra in Fig. 3f point out that this detection of UA could be performed not only in sweat but also in other solutions such as water and PBS. Compared with recent work on SERS detection of analyte in sweat (shown in Table S2†), these experimental data indicate that this wearable platform has excellent performance for SERS detection of UA in human sweat with complex components and in ambient environments.

3.4 Stretchability, flexibility, stability, and application of the wearable intelligent sweat platform

This paper presents a flexible and ultra-thin wearable sweat platform encapsulated with a soft, stretchable double-sided adhesive (300 μm thick) and PDMS (160 μm thick). This provides flexibility and stretchability to the wearable sweat platform. Fig. 4(a–c) illustrate the wearable sweat platform at different levels of bending, with the platform secured between the tips of forceps and subjected to various bending degrees by applying pressure. To better represent the bending degree of the wearable sweat platform, red pentagrams are used in Fig. 4(a–c), where three pentagrams in Fig. 4(c) signify the complete bending of the platform. Additionally, SERS spectra were collected under different bending conditions. As shown in Fig. 4(d), the SERS intensity of UA exhibited a variation of 9–15% under different bending conditions, indicating the excellent flexibility of the wearable sweat platform. During physical activity or daily movements, the human skin undergoes stretching, twisting, and deformation. A sensing platform needs to possess certain stretchability to maintain signal stability and accuracy. Evaluating the stretchability of a wearable sweat platform allows for the assessment of its durability and reliability, ensuring that it remains intact and functional under long-term use and different strain conditions. Pink pentagrams were used in Fig. 4(e–g) to indicate the degree of stretching (10–30%) of the wearable sweat platform, whereas three pentagrams in Fig. 4(h) indicate that the platform is largely stretched. SERS spectra were also collected for different stretching conditions. To investigate the impact of repeatability on the wearable sweat platform, this study conducted repeated stretching and bending tests 10, 30, and 50 times, resulting in a total collection of 180 SERS spectra for analysis. The research findings indicate that different numbers of stretching cycles may slightly influence the SERS signal, as varying stretching cycles could potentially affect the morphology, molecular structure, and optical properties of the wearable sensor, consequently leading to changes in the SERS spectra, as shown in Fig. S11(a–h).†

To demonstrate the utility of the device, we evaluated the performance of a wearable sweat platform for sweat collection and analysis in healthy humans. The device can be easily

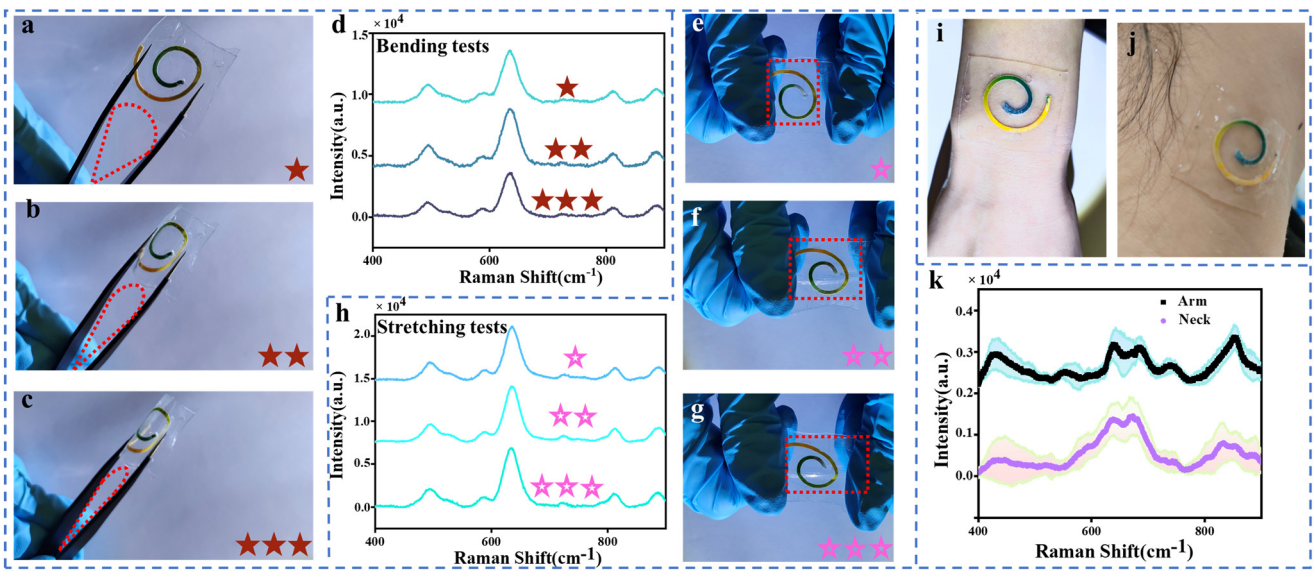

Fig. 4 Sweat platform flexibility, stretchability, and stability. Photographs of the sweat platform: (a) slightly twisted, (b) overly twisted, (c) fully twisted; (d) SERS spectra of UA collected at different degrees of bending. Photographs of the sweat platform (e) under 10% stretch, (f) under 20% stretch, (g), and under 30% stretch; (h) SERS spectra of UA collected at different degrees of stretch. Photographs of the sweat platform conformally laminated on the human subject: (i) the arm and (j) the neck. (k) SERS spectrum of the sweat collected from the arm and neck.

applied and comfortably worn anywhere on the body due to its soft mechanics, and the flexible and stretchable design accommodates skin deformations without device delamination and the limitations of natural body movement (Fig. 4i and j). We collected SERS spectra of sweat from a healthy human (Fig. 4k) who wore the device on the forearm and neck. The subject did not experience any skin irritation or discomfort during wear or after the device was removed.

3.5 Qualification of volume and pH of sweat

The collected sweat is analyzed using a smartphone to qualify the pH value and volume of sweat in this work. The pH indicator transitions to a deeper shade of blue as the pH value increases, which enables visual estimation of the pH value as shown in Fig. 5a. Fig. 5b displays the paper microfluidic channel in response to different pH values. The channel changes color from yellow at pH 3.8 to green and then blue as the pH value increases. A Python code is developed to analyze the color intensity of the paper microfluidic channel and extract images for further analysis. The code is designed to accurately recognize the color intensity of the paper microfluidic channel and provide an accurate pH value and volume of sweat. The corresponding Hue values are plotted in Fig. 5b and the Hue value increases with an increase of pH value.

The spiral paper serves as an efficient fluidic channel for transporting sweat and capturing UA with the help of capillary action. Fig. 5a shows 1 μL and 2.5 μL of synthetic sweat dripped on the wearable sweat platform, in which the travel distance of sweat is 34.81 mm and 50.56 mm with the channel width at 2 mm. To calculate the travel distance, the following equation can be used:

$$\text{Travel distance} = \frac{(\theta_1 \times R_1 \times \pi)(\theta_2 \times R_2 \times \pi)(\theta_3 \times R_3 \times \pi)}{180}$$

Here θ_1 and R_1 are the central angle and radius of the innermost half circle; θ_2 and R_2 are the central angle and radius of the second half circle; θ_3 and R_3 are the central angle and radius of the outermost half circle. Fig. 5c shows the structure parameter of the spiral paper, which includes the angle of the spiral channel. A Python code is developed to calculate the travel distance of sweat for automatic qualification of the angle. The code is capable of qualifying the angle of the spiral channels and calculating the travel distance of sweat by utilizing the structural parameters of the spiral paper. The details of qualification of the volume and pH value of sweat are described in Fig. S12 and S13.† Fig. 5d and S14† show the relationship between the calculated volume and travel distance of sweat. The red line corresponds to the results obtained from automatic qualification, whereas the green line represents the outcomes of manual measurement. Since these results generated from the above two methods are slightly deviated, the automatic qualification of the volume and pH value of sweat by the

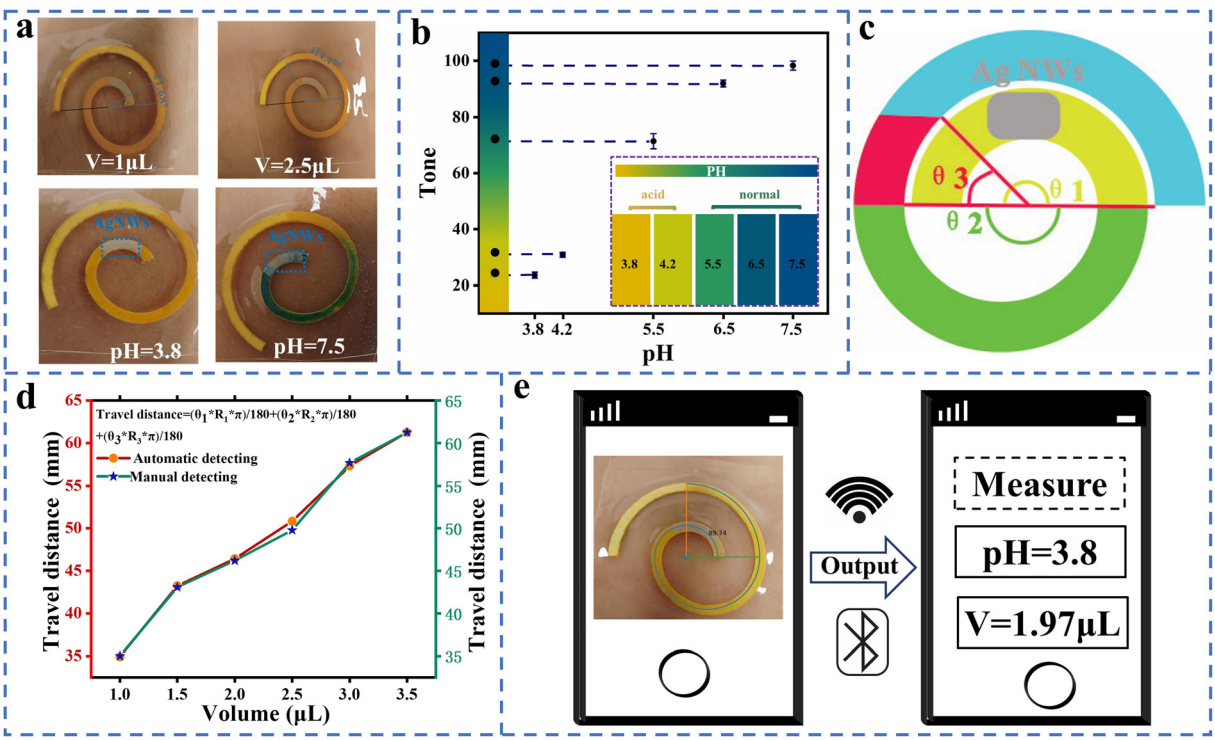

Fig. 5 (a) The photographs of the wearable platform on human skin. (b) The Hue value extracted from the wearable platform. (c) The structure parameter of the spiral channel. (d) The volume of sweat as a function of the travel distance. (e) Intelligent qualification of the volume and pH value of sweat.

smartphone is reliable in the application of this wearable intelligent sweat platform, whose process of qualification and interface are presented in Fig. 5e.

3.6 AI analysis for diagnosis of gout

An AI algorithm is adopted to analyze SERS spectra collected from human sweat for diagnosis of gout, whose process can be seen in Fig. 6a. Here the human sweat samples are collected from healthy persons. To simulate gout patients, some of these samples are spiked with UA at different concentrations.[22] In this work, several AI algorithms including PCA, PLS, and ANN are investigated to analyze SERS spectra of human sweat. PCA is a widely used algorithm for dimensionality reduction, compressing high-dimensional datasets into a lower-dimensional space by creating a new coordinate system that maximizes data variance. It eliminates noise and redundant information, improving data processing efficiency and reducing machine learning model complexity to mitigate overfitting. However, PCA assumes strict data distribution and may lead to information loss during dimensionality reduction. The PCA can reduce the dimensionality of large data sets but fails to analyze the SERS spectra of human sweat, as shown in Fig. 6b, which achieves the identification of gout with accuracy at 71% (Fig. S15a†). This work also used PLS to analyze the SERS spectra of human sweat. PLS is a regression algorithm that constructs a model depicting the relationship between input and output variables by decomposing the covariance matrix. It handles high-dimensional datasets effectively, does not assume specific data distributions, and addresses multicollinearity issues. However, it may exhibit constraints with nonlinear problems and requires parameter adjustments. The results point out that the SERS spectra of simulated gout were poorly identified in the PLS algorithm with an accuracy of only 79% as shown in Fig. 6c and S15b.† Besides, this work developed an optimized ANN algorithm to analyze the SERS spectra of human sweat. ANN emulates human brain neuron connectivity to classify and predict input data. It excels at addressing nonlinear problems, is versatile across different data types, and facilitates end-to-end model training without manual feature extraction. Fig. 6d and S16a† indicate that the ANN algorithm outperforms those traditional AI algorithms for identification of gout based on SERS spectra of human sweat. Furthermore, our data demonstrate that the identification accuracy of gout based on deep learning assisted SERS spectra collected in human sweat is obviously different in gender. Fig. 6e and f show that the ANN algorithm could achieve identification of gout with accuracy at 93%, 97%, and 88% for gout patients in various genders. The difference between single gender and mixed gender may come from the variations of components in sweat between male and female.[32] The main features and performance metrics of these sensors, including detection limits, are discussed. In addition, this work compares the performance of the SERS sweat platform in terms of these metrics with the results reported in other studies. These advantages make it suitable for real-time and accurate monitoring of target analytes in sweat, as shown in Tables S1 and S2.† Therefore, the combination of the AI algorithm

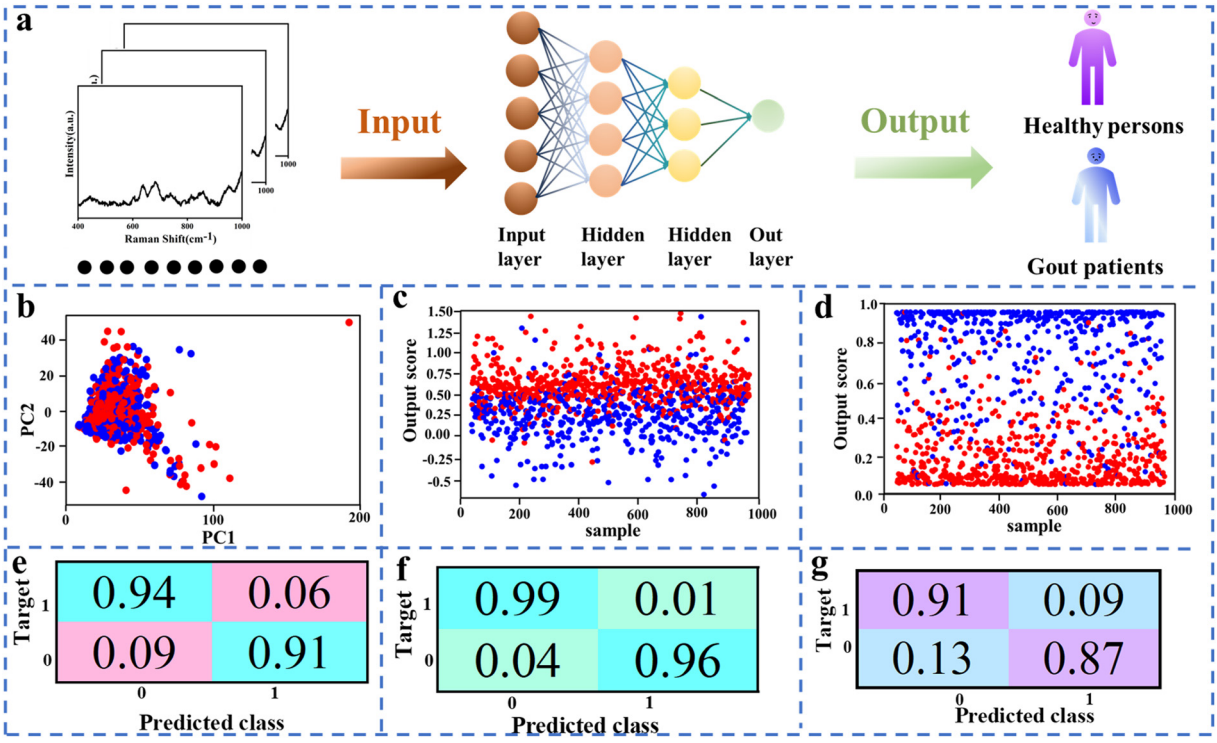

Fig. 6 (a) The process of AI analysis. (b–d) A two-dimensional LDA, PLS, and ANN score plot. (e–g) Prediction performance of male patients, female patients, and all patients.

and SERS spectra analysis has exhibited excellent potential in diagnosis of gout.

4. Conclusions

In conclusion, a wearable and visualized SERS platform enables the sensitive detection of UA in sweat at concentration as low as 0.1 μM. Additionally, with the help of photos from a smartphone, the volume and pH value of sweat could be quantified intelligently based on image recognition techniques. To diagnose gout, three AI algorithms were established based on sweat SERS spectra. The results show that the ANN algorithm achieves identification of gout at a high prediction accuracy of 97%. This work highlights the potential of SERS-AI in a wearable intelligent sweat platform for comfortable and noninvasive health diagnosis and explores research on sweat analysis.

Author contributions

Zhaoxian Chen: conceptualization, methodology, data curation, visualization, writing – original draft, and writing – review & and editing. Wei Wang, Hao Tian, and Xueli Zheng: software, visualization and data curation. Wenrou Yu: software, formal analysis. Yu Niu: resources. Shihong Liu and Li Wang: conceptualization and supervision. Yingzhou Huang: conceptualization, methodology, validation, writing – review & editing, and supervision.

Conflicts of interest

There are no conflicts to declare.

Acknowledgements

This research was supported by the National Natural Science Foundation of China (12374342 and 12074054), Chongqing Medical Scientific Research Project (Joint Project of Chongqing Health Commission and Science and Technology Bureau, 2023QNXM018), Chongqing Shapingba District Joint Project of Health Commission and Science and Technology Bureau (2023SOKWLH008) and the Sharing Fund of Chongqing University's Large-scale Equipment.

References

1 Y. Zang, F. Zhang, C. A. Di and D. Zhu, *Mater. Horiz.*, 2015, **2**, 140–156.
2 E. Roh, B. U. Hwang, D. Kim, B. Y. Kim and N. E. Lee, *ACS Nano*, 2015, **9**, 6252–6261.
3 S. Emaminejad, W. Gao, E. Wu, Z. A. Davies, H. Y. Y. Nyein, S. Challa, S. P. Ryan, H. M. Fahad, K. Chen, Z. Shahpar, S. Talebi, C. Milla, A. Javey and R. W. Davis, *Proc. Natl. Acad. Sci. U. S. A.*, 2017, **114**, 4625–4630.
4 X. Wang, Z. Liu and T. Zhang, *Small*, 2017, 13.
5 W. Tao, T. Liu, R. Zheng and H. Feng, *Sensors*, 2012, **12**, 2255–2283.
6 S. Kodama, K. Saito, Y. Yachi, M. Asumi, A. Sugawara, K. Totsuka, A. Saito and H. Sone, *Diabetes Care*, 2009, **32**, 1737–1742.
7 R. Ghaffari, D. S. Yang, J. Kim, A. Mansour, J. A. Wright, J. B. Model, D. E. Wright, J. A. Rogers and T. R. Ray, *ACS Sens.*, 2021, **6**, 2787–2801.
8 Y. Yang, Y. Song, X. Bo, J. Min, O. S. Pak, L. Zhu, M. Wang, J. Tu, A. Kogan, H. Zhang, T. K. Hsiai, Z. Li and W. Gao, *Nat. Biotechnol.*, 2020, **38**, 217–224.
9 F. Cui, Y. Yue, Y. Zhang, Z. Zhang and H. S. Zhou, *ACS Sens.*, 2020, **5**, 3346–3364.
10 J. Kim, S. Imani, W. R. de Araujo, J. Warchall, G. Valdés-Ramírez, T. R. L. C. Paixão, P. P. Mercier and J. Wang, *Biosens. Bioelectron.*, 2015, **74**, 1061–1068.
11 J. Xiao, Y. Luo, L. Su, J. Lu, W. Han, T. Xu and X. Zhang, *Anal. Chim. Acta*, 2022, 339843.
12 X. Wei, M. Zhu, J. Li, L. Liu, J. Yu, Z. Li and B. Ding, *Nano Energy*, 2021, **90**, 106031.
13 V. Patel, D. Saha, P. Kruse and P. R. Selvaganapathy, *ACS Appl. Nano Mater.*, 2022, **5**, 3957–3966.
14 X. Yang, J. Yi, T. Wang, Y. Feng, J. Wang, J. Yu, F. Zhang, Z. Jiang, Z. Lv, H. Li, T. Huang, D. Si, X. Wang, R. Cao and X. Chen, *Adv. Mater.*, 2022, **33**, 2201768.
15 Z. Xu, J. Song, B. Liu, S. Lv, F. Gao, X. Luo and P. Wang, *Sens. Actuators, B*, 2021, **348**, 130674.
16 X. Xie, N. Gao, Y. Huang and Y. Fang, *ACS Appl. Mater. Interfaces*, 2022, **14**, 51468–51475.
17 S. Schlücker, *Angew. Chem., Int. Ed.*, 2014, **53**, 4756–4795.
18 J. Langer, D. J. de Aberasturi, J. Aizpurua, R. A. Alvarez-Puebla, B. Auguié, J. J. Baumberg, G. C. Bazan, S. E. J. Bell, A. Boisen, A. G. Brolo, J. Choo, D. Cialla-May, V. Deckert, L. Fabris, K. Faulds, F. Javier García de Abajo, R. Goodacre, D. Graham, A. J. Haes, C. L. Haynes, C. Huck, T. Itoh, M. Käll, J. Kneipp, N. A. Kotov, H. Kuang, E. C. Le Ru, H. K. Lee, J. F. Li, X. Y. Ling, S. A. Maier, T. Mayerhöfer, M. Moskovits, K. Murakoshi, J. M. Nam, S. Nie, Y. Ozaki, I. Pastoriza-Santos, J. Perez-Juste, J. Popp, A. Pucci, S. Reich, B. Ren, G. C. Schatz, T. Shegai, S. Schlücker, L. L. Tay, K. George Thomas, Z. Q. Tian, R. P. van Duyne, T. Vo-Dinh, Y. Wang, K. A. Willets, C. Xu, H. Xu, Y. Xu, Y. S. Yamamoto, B. Zhao and L. M. Liz-Marzán, *ACS Nano*, 2020, **14**, 28–117.
19 H. Chen, S. G. Park, N. Choi, H. J. Kwon, T. Kang, M. K. Lee and J. Choo, *ACS Sens.*, 2021, **6**, 2378–2385.
20 H. Lai, G. Li, F. Xu and Z. Zhang, *J. Mater. Chem. C*, 2020, **8**, 2952–2963.
21 X. Xie, Y. Zhang, L. Zhang, J. Zheng, Y. Huang and H. Fa, *Anal. Chem.*, 2021, **93**, 13219–13225.
22 H. S. Kim, H. J. Kim, J. Lee, T. Lee, J. Yun, G. Lee and Y. Hong, *Anal. Chem.*, 2021, **93**, 14996–15004.
23 M. Chung, W. H. Skinner, C. Robert, C. J. Campbell, R. M. Rossi, V. Koutsos and N. Radacsi, *ACS Appl. Mater. Interfaces*, 2021, **13**, 51504–51518.
24 Y. Wang, C. Zhao, J. Wang, X. Luo, L. Xie, S. Zhan, J. Kim, X. Wang, X. Liu and Y. Ying, *Sci. Adv.*, 2021, **7**, eabe4553.
25 U. Mogera, H. Guo, M. Namkoong, M. S. Rahman, T. Nguyen and L. Tian, *Sci. Adv.*, 2022, **8**, abn1736.

26 X. Lin, D. Lin, Y. Chen, J. Lin, S. Weng, J. Song and S. Feng, *Adv. Funct. Mater.*, 2021, **31**, 2103382.
27 X. Ren, W. Nam, P. Ghassemi, J. S. Strobl, I. Kim, W. Zhou and M. Agah, *Microsyst. Nanoeng.*, 2022, **6**, 255–265.
28 H. Shin, S. Oh, S. Hong, M. Kang, D. Kang, Y. G. Ji, B. H. Choi, K. W. Kang, H. Jeong, Y. Park, H. K. Kim and Y. Choi, *ACS Nano*, 2020, **14**, 5435–5444.
29 Y. Sun and Y. Xia, *Adv. Mater.*, 2002, **14**, 833–837.
30 L. Zhang, J. Sun, Z. Li, Y. Yuan, A. Liu and Y. Huang, *ACS Appl. Mater. Interfaces*, 2020, **12**, 32746–32751.
31 S. R. Sahoo, S. Huey-Jen Hsu, D. A. Chou, G. J. Wang and C. C. Chang, *Biosens. Bioelectron.*, 2022, **213**, 114440.
32 A. V. Patel and A. L. Gaffo, *J. Inflammation Res.*, 2022, **15**, 1591–1598.